Electrolytes for Zn Batteries

Deep Eutectic Solvents in Polymer Gels

Gregorio, Victor; Jankowski, Piotr; Garcia, Nuria; Lastra, Juan Maria Garcia; Tiemblo, Pilar; Chang, Jin Hyun

Published in:
ChemSusChem

Link to article, DOI:
10.1002/cssc.202300256

Publication date:
2023

Document Version
Publisher's PDF, also known as Version of record

ChemSusChem

Research Article
doi.org/10.1002/cssc.202300256

Chemistry Europe
European Chemical Societies Publishing

www.chemsuschem.org

Special Collection

Electrolytes for Zn Batteries: Deep Eutectic Solvents in Polymer Gels

Victor Gregorio,*[a, b] Piotr Jankowski,[b, c] Nuria Garcia,[a] Juan Maria Garcia Lastra,[b] Pilar Tiemblo,[a] and Jin Hyun Chang*[b]

Gel polymer electrolytes composed of deep eutectic solvent acetamide$_4$:Zn(TFSI)$_2$ and poly(ethylene oxide) (PEO) are prepared by using a fast, solvent-free procedure. The effect of the PEO molecular weight and its concentration on the physicochemical and electrochemical properties of the electrolytes are studied. Gels prepared with ultrahigh molecular-weight PEO present pseudo-solid behavior and ionic conductivity even higher than that of the original liquid electrolyte. A decrease in the dendritic growth in soft gels with PEO contents up to 1 wt% is demonstrated. The changes in the chemical structure of the electrolyte produced by the strong interactions between ethylene oxide units and Zn^{2+} have also been studied. The addition of PEO takes the electrolyte out of its original eutectic composition, producing blend crystallization. However, it is possible to retain the eutectic point of the electrolyte in a gel form if the addition of PEO is accompanied by the reduction of acetamide.

Introduction

The global demand for energy storage has grown exponentially since the discovery of lithium-ion batteries,[1,2] which is due not only to the development of portable electronic devices but also to the emergence of electric vehicles[3] and the necessity of large-scale stationary energy storage for intermittent renewable energy sources.[4] Lithium is a scarce element on earth and is not geographically evenly distributed.[5,6] Therefore, alternative chemistries to lithium-ion technology will play a key role in future sustainability.[7] In this regard, there are important efforts to develop batteries based on different metals such as Na, Mg, Al, or Zn.[8–10] In that context, a Zn-based battery is an attractive alternative, owing to zinc's large volumetric capacity, abundance, and superior safety compared to lithium and other metals.[11,12] However, the use of common corrosive alkaline electrolytes leads to dendrite growth and soluble ZnO_2^{2-} formation on the Zn anode.[13,14] Consequently, a switch to a nonaqueous solution was suggested, which induces a change in its working mechanism towards the "rocking chair" type where Zn^{2+} ions migrate between the two electrodes.[15]

Initially, electrolytes based on room temperature ionic liquids (RTILs), such as [EMIm][TFSI] (1-ethyl-3-methylimidazolium bis(trifluoromethanesulfonyl)imide) and [BMIm][TFSI] (1-butyl-3-methylimidazolium bis(trifluoromethanesulfonyl)imide), attracted interest due to their negligible vapor pressure, high ionic conductivity, and high thermal and electrochemical stability.[16,17] However, their high cost nullifies the advantage of the low-cost Zn anodes. Another type of solvent has recently gained attention as an alternative to conventional RTILs: deep eutectic solvents (DESs).[18] They are usually created from two or three nontoxic and environmentally benign components, which can self-organize through hydrogen bond interactions to form a eutectic mixture with a melting point significantly lower than those of their components. The characteristics of DESs are mostly controlled by the structures of constituent components, which can be tailored to specific chemistry or application. Despite their versatility, DESs have common properties such as decreased vapor pressure and toxicity, high metal solubility, easy preparation, and low cost.[19] Several Zn DES have been reported to date:[20] choline chloride/urea or ethylene glycol with $ZnCl_2$,[21] acetamide (ACE) with either $Zn(ClO_4)_2$[22] or $Zn(TFSI)_2$.[23] All these DESs are comparatively cheap, nonflammable, and exhibit low vapor pressure. When used as electrolytes, they have proved to be able to deposit Zn on electrode surfaces[22] and to intercalate it in MnO_2 cathodes.[24] The DESs based on Zn(TFSI)$_2$-acetamide mixture are especially attractive for battery applications as they generate in-situ solid electrolyte interphase, increasing electrode efficiency and battery lifetime.[23] However, the growth of dendrites is still an urgent

[a] V. Gregorio, Dr. N. Garcia, Dr. P. Tiemblo
Instituto de Ciencia y Tecnología de Polímeros
Consejo Superior de Investigaciones Científicas (ICTP-CSIC)
Calle Juan de la Cierva 3, 28006 Madrid (Spain)
E-mail: victgr@dtu.dk
[b] V. Gregorio, Dr. P. Jankowski, Prof. J. M. Garcia Lastra, Prof. J. H. Chang
Department of Energy Conversion and Storage
Technical University of Denmark
Anker Engelunds vej, Building 301, 2800 Kongens Lyngby (Denmark)
E-mail: jchang@dtu.dk
[c] Dr. P. Jankowski
Faculty of Chemistry, Warsaw University of Technology (WUT)
Warsaw, 00-661 Poland

Supporting information for this article is available on the WWW under https://doi.org/10.1002/cssc.202300256

This publication is part of a Special Collection on Battery Research in Europe jointly organized by Battery 2030+ and Chemistry Europe. It features contributions in the framework of Battery 2030+ from scientists throughout Europe.

issue, and further research is needed to suppress its nucleation and growth effectively.

Tuning the electrolyte consistency was shown to be one of the possible ways of dendrite suppression.[25,26] Using polymer-based solid, quasi-solid, or gel electrolytes prevents leaks and suppresses dendritic growth. However, adding a polymer to a liquid electrolyte may decrease the ionic conductivity significantly, which is particularly detrimental for the Zn-containing DESs as their ionic conductivity is already rather low. Moreover, there was a period in which researchers assumed that inhibiting dendrites involved creating a mechanical resistance to their growth,[27,28] i.e., the polymer electrolytes needed to show relatively high elastic modulus to stop dendrites, consequently lowering the ion mobility substantially.[26]

However, in 2014, Archer and co-workers reported a chemically-crosslinked polymer gel electrolyte with a low elastic modulus that can suppress dendrites in a Li cell.[29] The work on the effect of adding a low concentration of polymers to electrolytes on dendrite suppression has been reported for different metal electrodes since 2018.[29] In 2019, the same authors reported on the electrochemical performance of ultra-high molecular weight (UHMW) poly(methyl methacrylate) (PMMA) and organic liquid electrolytes (propylene and ethylene carbonate, dimethyl sulfoxide) containing Li, Na, Zn, and Cu salts.[30] They produced viscoelastic gels while keeping the UHMW polymer concentration under around 1 wt% such that its impact on the ionic conductivity is negligible. Homogeneous electrodeposition of metallic cations without dendrite formation was observed when these gels were used, which is attributed to the reduction of electroconvection in gel electrolytes compared to their liquid counterparts.

An increased homogeneity in electrodeposition has been observed for other battery systems when polymer gels are employed: K-based[31] cell with polyvinylidene difluoride (PVDF) gels reinforced with polyacrylonitrile (PAN) fibers and Mg-based[32] cell with in-situ polymerized poly(tetrahydrofuran). For the case of Zn-based cells, using polymers such as polyethylene glycol (PEG),[33] polyacrylamide,[34] poly(acrylic acid) and poly(vinyl alcohol) electrolyte,[35] and poly(ethylene oxide) (PEO)[35] with an average molecular weight of 100000 g mol^{-1} as an additive in aqueous Zn electrolytes has shown to inhibit the dendritic growth on Zn anodes and prolong the lifetime of the cells.[25]

It is worth noting that dendritic growth in Zn-based cells is suppressed for both PEO with an average molecular weight of 100000 g mol^{-1}[25] and UHMW PMMA despite their different influence on the ionic conductivity; the ionic conductivity is decreased for PEO[32] while it remains unchanged for UHMW PMMA.[29] These results suggest the potential benefits of incorporating UHMW polymer gel electrolytes in Zn batteries as they can help to mitigate the dendrite growth without reducing the ionic conductivity. UHMW PEO is soluble under certain conditions in a wide variety of metal cation electrolytes,[36,37] including Al, Na and Li DESs and RTILs, making it possible to prepare polymer gels with very low PEO concentrations without introducing any auxiliary solvents.

In this work, gels consisting of eutectic acetamide and zinc bis(trifluoromethanesulfonyl)imide ($Zn(TFSI)_2$) mixture and PEO have been prepared while varying PEO molecular weight and concentration, and the acetamide/$Zn(TFSI)_2$ ratio. Their rheology, chemical structure, and phase transitions have been studied to understand the impact of the PEO concentration and molecular weight on the eutectic equilibrium of the DESs and the ionic conductivity. Subsequently, dendrite mitigation, cycling performance, and reversibility have been studied for selected gels. We found that the gels prepared with UHMW PEO at low concentrations show higher ionic conductivity and strong dendrite suppression than the liquid DES.

Results and Discussion

Two sets of blends are prepared, and their glass transition temperature (T_g), ionic conductivity (σ), and rheological properties are studied. First, blends are prepared by adding 1 wt% of PEO to $ACE_4Zn(TFSI)_2$ (corresponding molar ratio of $ACE_4PEO_{0.2}Zn(TFSI)_2$) with different molecular weights (MW) to investigate the impact of the PEO presence and its MW variation. Subsequently, the second batch of gel electrolytes with a varying molar ratio between ACE, PEO, and $Zn(TFSI)_2$ was compared to understand the effect of their relative concentrations.

Formation of the gel network in the eutectic $ACE_4Zn(TFSI)_2$ with 1 wt% PEO

Gel electrolytes are made by adding 1 wt% PEO of varying MW to $ACE_4Zn(TFSI)_2$. Three different MW of PEO, 100000, 900000, and 5000000 g mol^{-1}, are studied, and these samples are denoted as $ACE_4PEO_{0.2}Zn(TFSI)_2$-1, $ACE_4PEO_{0.2}Zn(TFSI)_2$-9, $ACE_4PEO_{0.2}Zn(TFSI)_2$-50, respectively. The suffix in the name corresponds to the MW of PEO in 100000 g mol^{-1}. The effects of PEO and its MW variation on T_g, σ, and rheological properties of $ACE_4Zn(TFSI)_2$ are shown in Table 1. $ACE_4PEO_{0.2}Zn(TFSI)_2$-50 presents the highest ionic conductivity, even higher than that of the liquid electrolyte while having the most solid-like character, which is represented by the low crossover frequency between the storage modulus (G') and the loss modulus (G''). It is also interesting to note that both the conductivity and viscosity increase as the MW is increased, which presents the potential to develop solid and quasi-solid electrolytes with good mechanical and electrochemical properties.

The physicochemical properties of these electrolytes are shown in Figure 1. The differential scanning calorimetry (DSC) scans in Figure 1a show the phase transitions and relaxations of $ACE_4Zn(TFSI)_2$ and its blends with PEO. The first heating scans (solid lines) show the melting of crystalline species at 54 °C in the blends of $ACE_4Zn(TFSI)_2$ with PEO, although liquid $ACE_4Zn(TFSI)_2$ has no transitions above its T_g, which is observed at −37.5 °C. This result reveals that PEO is not an inert component in the blend. PEO is known to interact with ACE[38] and also with Zn^{2+} ion when PEO is mixed with zinc chloride,[39] zinc bromide

Table 1. T_g, σ, Newtonian viscosity (η_0), plateau storage modulus (G_0^N), and crossover ($G' = G''$) of $ACE_4Zn(TFSI)_2$ and its blends with 1 wt% PEO of different MW.

Sample	T_g [°C]	$\sigma \cdot 10^3$ [S cm^{-1}] 40 °C	60 °C	Rheology at 60 °C η_0 [Pa s]	G_0^N [Pa]	$G' = G''$ [rad s^{-1}]
$ACE_4Zn(TFSI)_2$	−37.5	0.37	0.99	–	–	–
$ACE_4PEO_{0.2}Zn(TFSI)_2$-1	−37.0	0.60	1.70	0.45	–	>100
$ACE_4PEO_{0.2}Zn(TFSI)_2$-9	−37.0	0.57	1.65	29.0	–	>100
$ACE_4PEO_{0.2}Zn(TFSI)_2$-50	−37.0	0.77	2.25	315	60	0.60

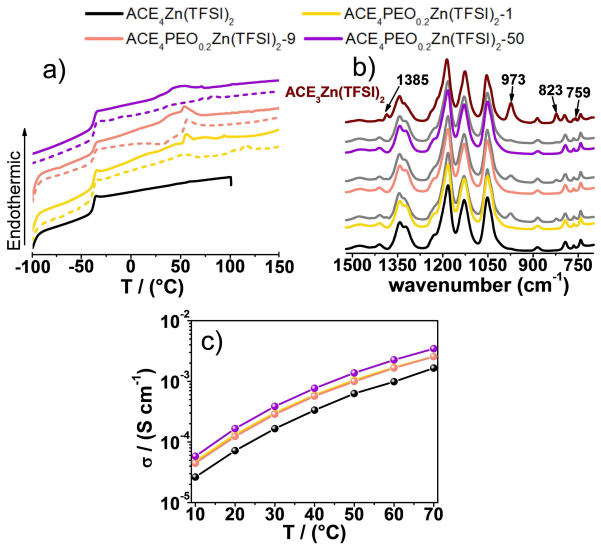

Figure 1. Physicochemical properties of gel electrolytes with 1% PEO of different chain lengths: a) First (solid line) and second (dotted line) DSC heating scans. b) FTIR spectra from 700 to 1500 cm^{-1} recorded on freshly prepared gels (color lines) and after 15 days (gray lines) $ACE_4Zn(TFSI)_2$ in black and $ACE_3Zn(TFSI)_2$ in red are added for comparison. c) Ionic conductivity at temperatures between 10 °C and 70 °C. The $ACE_4PEO_{0.2}Zn(TFSI)_2$-1 curve in (c) is not clearly visible since it almost coincides with the curve of $ACE_4PEO_{0.2}Zn(TFSI)_2$-9.

complexes[40] and aqueous solutions containing zinc acetate and zinc chloride.[41] The interaction of PEO with DES shifts the DES formulation away from its eutectic point where it is fully liquid, inducing the coexistence of liquid and crystalline phases. The melting endotherm at 54 °C in the first scan of the blends is smaller in the second heating scan (dotted lines) or even absent for $ACE_4PEO_{0.2}Zn(TFSI)_2$-50. This trend suggests that the phase separation and crystallization produced by the incorporation of PEO is slowed down by viscosity, which is particularly high in $ACE_4PEO_{0.2}Zn(TFSI)_2$-50.

The Fourier transform infrared (FTIR) spectra of the three gel samples are collected immediately after the gel processing and 15 days later to study the speciation changes in the DESs upon the addition of PEO and the possible kinetic effects of the PEO MW (Figure 1b and Figure S2 in the Supporting Information). The spectra for $ACE_4Zn(TFSI)_2$ and $ACE_3Zn(TFSI)_2$ are also included for a comparison with eutectic and noneutectic mixtures, respectively. The FTIR spectra of fresh gels, very similar to that of $ACE_4Zn(TFSI)_2$ do not show bands at 758, 823, 973, and 1385 cm^{-1}. However, all these four bands present in the noneutectic mixture $ACE_3Zn(TFSI)_2$ show up as peaks in $ACE_4PEO_{0.2}Zn(TFSI)_2$-1 and $ACE_4PEO_{0.2}Zn(TFSI)_2$-9 gels after 15 days. For the $ACE_4PEO_{0.2}Zn(TFSI)_2$-50 gel, the vibrations at 823 and 973 cm^{-1} appear only as shoulders, whereas the vibrations at 758 and 1385 cm^{-1} do not appear. This suggests that these bands are related to crystalline species formed after the gels are cooled down to room temperature (RT) at different rates depending on the environment viscosity (i.e., depends on the molecular weight of PEO). The FTIR and DSC results agree very well, proving that adding a small concentration of PEO to $ACE_4Zn(TFSI)_2$ induces a phase separation in the DESs, whose rate depends on the viscosity of the blend. The phase separation rate is the slowest for the $ACE_4PEO_{0.2}Zn(TFSI)_2$-50 sample with the highest viscosity.

The ionic conductivity (σ) of all electrolytes follows the Vogel-Fulcher-Tammany model where lnσ decreases linearly when plotted as a function of $\frac{1}{(T-T_0)}$, which is a characteristic of viscous liquids (Figure S3). Remarkably, the ionic conductivity of the three gels is higher than that of the pure DESs for all the temperatures measured (Figure 1c and Table S1). Moreover, the highest σ is observed for the $ACE_4PEO_{0.2}Zn(TFSI)_2$-50 sample produced with PEO with the highest MW (5000000 g mol^{-1}). The $ACE_4PEO_{0.2}Zn(TFSI)_2$-1 and $ACE_4PEO_{0.2}Zn(TFSI)_2$-9 samples have very similar conductivity values that are higher than the original $ACE_4Zn(TFSI)_2$. This phenomenon has been previously reported[37] and is attributed to the combination of the chemical and the rheological effects of the polymer on the DES. The chemical effects depend on the PEO concentration but not on its MW, whereas the rheological effects depend also on the MW of the polymer. There is an uncoupling of η_0 and ionic mobility for gels with a low concentration of very long polymer chain (i.e., ionic conductivity remains similar to that of the liquid media while viscosity is increased dramatically).[30] If the changes in the chemical structure of DESs induced by the presence of PEO render a liquid phase with higher ion mobility, the combination of chemical and rheological effects can result in gels with σ higher than the liquid electrolyte.

The chemical role of PEO is investigated using density functional theory (DFT) calculations. Figure 2 depicts the interaction of PEO with molecules present in DESs. The oxygen atoms in the polymer chain can coordinate Zn^{2+} cation and acetamide through the NH_2 group with the interaction strength of 59.1 kJ mol^{-1} and 25.1 kJ mol^{-1}, respectively. These values are comparable with other interactions present in DESs, namely those between acetamide and $TFSI^-$ anion or between two acetamide molecules, which are 29.6 kJ mol^{-1} and 36.3 kJ mol^{-1},

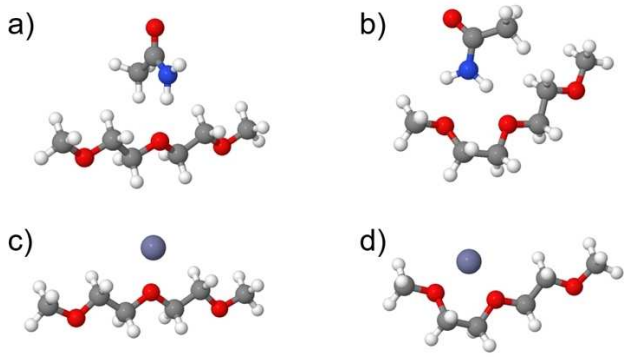

Figure 2. Optimized geometries of a,b) acetamide and c,d) Zn^{2+} interacting with PEO chain.

respectively. However, these interactions are much weaker than the interaction between Zn^{2+} cation and $TFSI^-$ anion, which is 154.4 kJ mol^{-1}. Nonetheless, the energetic analysis indicates a high likelihood of the polymer chain participating in interactions with the DES species and cluster formation. The coordination of Zn^{2+} by single oxygen of PEO (Figure 2c; 59.1 kJ mol^{-1}) already indicates strong interaction. The wrapping of the flexible polymer chain around the cation increases the interaction to 147.6 kJ mol^{-1} when two oxygen centers are used (Figure 2d) and to 267.1 kJ mol^{-1} when Zn^{2+} is fully coordinated by four oxygen atoms. Any coordination of Zn^{2+} cations by O-centers shows a high thermodynamical preference, which reduces the concentration of available cation (hydrogen bond acceptor), whereas the less favored interaction of PEO with the NH_2 group of acetamide (Figure 2a; 25.1 kJ mol^{-1}) may reduce the concentration of hydrogen bond donor. Interestingly, the considered interaction of acetamide by neighboring oxygen atoms was found to be unstable (Figure 2b; −42.7 kJ mol^{-1}); thus, only docking of acetamide to a single O-center is possible.

The best combination of rheological properties and σ is obtained when UHMW PEO is used. These eutectogel electrolytes present σ significantly higher than that of $ACE_4Zn(TFSI)_2$ while behaving as a pseudo-solid material. Thus, we selected UHMW PEO for further studies. The suffix in the sample name (i.e., x in the sample name $ACE_4PEO_{0.2}Zn(TFSI)_2$-*x*) is omitted for the rest of this manuscript for simplicity, which implies that MW of 5000000 g mol^{-1} is used (equivalent to having a suffix of 50) unless it is explicitly stated.

A balance between ACE and PEO and its effect on rheology and ionic conductivity

The results reported in the previous section suggest that the presence of PEO can modify the properties of DES substantially because of its interaction with both Zn^{2+} and ACE. Thus, four new gel electrolytes with varying molar ratios between ACE and PEO are prepared. The physicochemical properties of these formulations and $ACE_4PEO_{0.2}Zn(TFSI)_2$ are shown in Table 2. Note that $ACE_4PEO_{0.5}Zn(TFSI)_2$ and $ACE_{3.5}PEO_{0.5}Zn(TFSI)_2$ gels correspond to an addition of 2.5 wt% PEO, and $ACE_4PEO_1Zn(TFSI)_2$ and $ACE_3PEO_1Zn(TFSI)_2$ gels correspond to an addition of 5 wt% PEO.

Figure 3 shows the effect of the different ACE/PEO ratios on the gel's speciation and its impact on thermal transitions, rheology, and ionic conductivity. Remarkably, only $ACE_4PEO_1Zn(TFSI)_2$ (5 wt% PEO) shows a significant melting endotherm. In contrast, no solid phases appear in $ACE_3PEO_1Zn(TFSI)_2$, when 5 wt% of PEO is added to produce the gel while the ACE content is decreased, suggesting the interaction between PEO and the different species in the eutectic formulation and producing phase segregation. Figures 3b and S4 present a comparison of the FTIR spectra of $ACE_4Zn(TFSI)_2$, $ACE_3Zn(TFSI)_2$ and $ACE_3PEO_1Zn(TFSI)_2$. As explained previously, the noneutectic mixture $ACE_3Zn(TFSI)_2$ presents four characteristic bands of solid precipitates at 759, 823, 973, and 1385 cm^{-1}. These bands are absent in $ACE_3PEO_1Zn(TFSI)_2$, and its spectra resemble those of the eutectic mixture $ACE_4Zn(TFSI)_2$, except for a small shoulder at 960 cm^{-1} that is characteristic of PEO. This result suggests that the strong interaction of PEO with the Zn species in ACE:$Zn(TFSI)_2$ mixtures can turn a noneutectic composition with a $Zn(TFSI)_2$ content above the eutectic region into an eutectogel, which does not show any signs of phase segregation.

Table 2. T_g, σ, and rheology of gel electrolytes prepared using PEO with MW of 5000000 g mol^{-1} with different ACE:PEO ratios.

Sample	PEO [wt%]	T_g [°C]	$\sigma\cdot10^3$ [S cm^{-1}] 40 °C	60 °C	Rheology (60 °C) $G'=G''$ [rad s^{-1}]	G_0^N [Pa]
$ACE_4Zn(TFSI)_2$	–	−37.5	0.37	0.99	–	–
$ACE_4PEO_{0.2}Zn(TFSI)_2$	1.0	−37.0	0.77	2.25	0.60	60
$ACE_4PEO_{0.5}Zn(TFSI)_2$	2.5	−35.5	0.62	1.88	0.03	700
$ACE_{3.5}PEO_{0.5}Zn(TFSI)_2$	2.5	−35.5	0.62	2.10	0.03	650
$ACE_3PEO_1Zn(TFSI)_2$	5.0	−34.4	0.46	1.62	<0.01	2350
$ACE_4PEO_1Zn(TFSI)_2$	5.0	−30.5	0.37	1.17	<0.01	3000

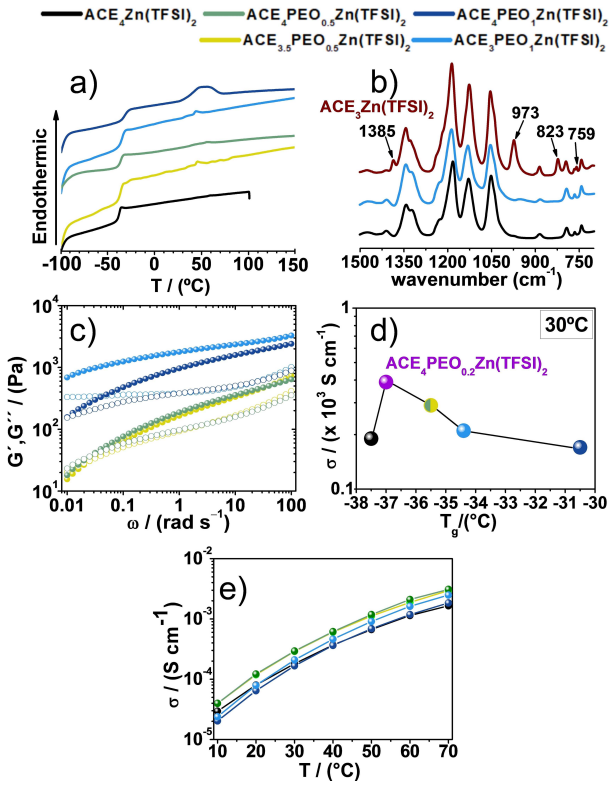

Figure 3. Physicochemical properties of $ACE_4Zn(TFSI)_2$ DESs and its gel electrolytes with different ACE:PEO ratios: a) First DSC heating scan. b) FTIR spectra from 700 to 1500 cm^{-1} of $ACE_3PEO_1Zn(TFSI)_2$ compared with its original liquid mixture $ACE_3Zn(TFSI)_2$ and the eutectic mixture $ACE_4Zn(TFSI)_2$. c) Rheology curves at 60 °C, where G' and G'' are shown in filled and unfilled circles, respectively. d) Conductivity at 30 °C as a function of T_g. e) Ionic conductivity at temperatures between 10 °C and 70 °C.

Figure 3c shows the rheology curves of the gels at 60 °C. The curves of $ACE_4PEO_{0.5}Zn(TFSI)_2$ and $ACE_{3.5}PEO_{0.5}Zn(TFSI)_2$ gels (both with 2.5 wt% PEO) are quite similar. However, a noticeable difference is observed when comparing $ACE_3PEO_1Zn(TFSI)_2$ and $ACE_4PEO_1Zn(TFSI)_2$ gels (both with 5 wt% PEO); the $ACE_4PEO_1Zn(TFSI)_2$ gel has a higher plateau storage modulus, a lower tan(δ) (determined by $\tan\delta = \frac{G''}{G'}$) and a lower crossover frequency than the $ACE_3PEO_1Zn(TFSI)_2$ gel. As the $ACE_4PEO_1Zn(TFSI)_2$ gel has a clear melting endotherm in the DSC scan (Figure 3a), the plateau storage modulus increases and the moduli crossover at a lower frequency can be explained by the presence of crystalline species in $ACE_4PEO_1Zn(TFSI)_2$. These crystals can act as crosslinking points, impeding mobility. The rheology curves at 80 °C of $ACE_4PEO_1Zn(TFSI)_2$ and $ACE_3PEO_1Zn(TFSI)_2$ are presented in Figure S6 in the Supporting Information to compare these two samples above the melting point of all the crystalline species. At 80 °C, both gels have similar rheological behavior; in fact, $ACE_3PEO_1Zn(TFSI)_2$ presents a moduli crossover at a lower frequency. The results indicate that decreasing the ACE content does not deteriorate the gel's rheological properties, suggesting that the elastic properties of the gel electrolytes rely strongly on the interactions between units of PEO and Zn^{2+} and not between ACE and Zn^{2+} or ACE and PEO.

Figure 3d illustrates the ionic conductivity at 30 °C as a function of the T_g of the gels in Table 2. The $ACE_4PEO_{0.2}Zn(TFSI)_2$ gel (1 wt% PEO) exhibits higher σ and T_g than those of the liquid DESs ($ACE_4Zn(TFSI)_2$). The ionic conductivity decreases progressively as the PEO concentration increases, in accordance with their increasing T_g. Gels with 2.5 wt% PEO have the same T_g of −35.5 °C and the same σ, indicating that these two formulations are very similar in terms of their microscopic mobility. However, a significant difference in the T_g and σ are seen for the gels with 5 wt% PEO; $ACE_3PEO_1Zn(TFSI)_2$ has lower T_g and consequently higher σ than $ACE_4PEO_1Zn(TFSI)_2$.

Figure 3e shows σ for temperatures between 10 °C and 70 °C and these σ values are also represented in Table S1. Again, the 2.5 wt% PEO gels ($ACE_{3.5}PEO_{0.5}Zn(TFSI)_2$ and $ACE_4PEO_{0.5}Zn(TFSI)_2$) display nearly identical σ for all considered temperatures, showing a similar temperature dependence of σ, and having their σ significantly higher than the original DESs without PEO. Such similarities of σ over a wide range of temperatures are not surprising as the T_g of both these 2.5 wt% eutectogels is the same. For the 5 wt% PEO gels, the dependence of σ on temperature is stronger for $ACE_3PEO_1Zn(TFSI)_2$ than for $ACE_4PEO_1Zn(TFSI)_2$, in agreement with their different T_g. The temperature dependence of σ is stronger than the liquid DESs for both 5 wt% PEO gels; σ of liquid DESs is the lowest of the three at 70 °C and the highest at 10 °C.

Effect of the polymer molecular weight on the electrochemical properties and dendrite suppression

A set of electrochemical characterization studies is performed to gain more insights into the viability of the polymer gels as electrolytes for Zn batteries. As a first step, gels with 1 wt% PEO (i.e., $ACE_4PEO_{0.2}Zn(TFSI)_2$-*x* samples where $x = 1$, 9 and 50) are studied in Zn||Zn symmetrical cells. As detailed in the experimental section, the cells are assembled without a separator; only a Teflon ring is employed to prevent the electrodes from touching another, allowing the dendritic growth between electrodes. Figure 4 shows the rheology curves of the $ACE_4PEO_{0.2}Zn(TFSI)_{2\text{-}x}$ gels (Figure 4a) and their stripping plating behavior in Zn||Zn symmetrical cells (Figure 4b) at 60 °C. The stripping−plating studies are conducted at 40 °C throughout this manuscript except for the $ACE_4PEO_{0.2}Zn(TFSI)_2$-*x* gels in Figure 4b as these samples present signs of crystallization around 50 °C (see DSC scan curves in Figure 1a). The rheology of the samples with low MW, $ACE_4PEO_{0.2}Zn(TFSI)_2$-1 and $ACE_4PEO_{0.2}Zn(TFSI)_2$-9, is liquid-like in the frequency range measured, where G'' is higher than G'. The sample with UHMW ($ACE_4PEO_{0.2}Zn(TFSI)_2$-50), on the other hand, presents a solid-like character until 0.6 rad s^{-1}.

The correlation between rheological properties and dendrite growth is quite apparent. The short-circuit of the cells occurs at a later stage of the stripping−plating cycles when the electrolytes exhibit a more solid-like character; the lifetime is the shortest for the liquid $ACE_4Zn(TFSI)_2$ (6 cycles), followed by

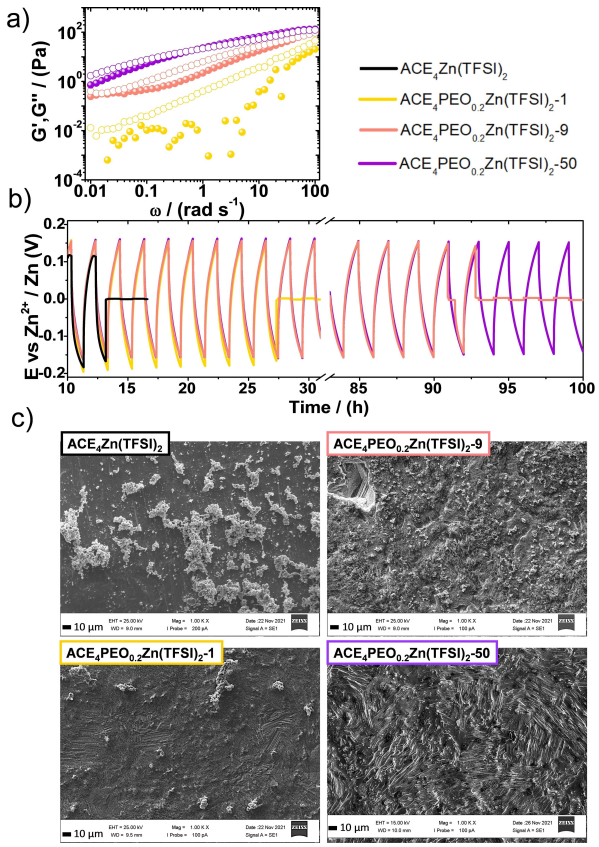

Figure 4. a) Rheology curves at 60 °C of $ACE_4Zn(TFSI)_2$ DESs and $ACE_4PEO_{0.2}Zn(TFSI)_{2\text{-}x}$ gels, G' (filled circles) and G'' (unfilled circles)- b) Stripping–plating behavior of $ACE_4Zn(TFSI)_2$ DESs and $ACE_4PEO_{0.2}Zn(TFSI)_{2\text{-}x}$ gels at 60 °C in Zn||Zn symmetrical cells. c) Surface of the electrodes analyzed by SEM after cycling.

$ACE_4PEO_{0.2}Zn(TFSI)_2$-1 (13 cycles) and $ACE_4PEO_{0.2}Zn(TFSI)_2$-9 (46 cycles). Finally, the $ACE_4PEO_{0.2}Zn(TFSI)_2$-50 sample with the loss and storage moduli crossover at 0.6 rad s^{-1} does not show a sign of a short-circuit within the 100 h of measurement duration. To better understand the effect of PEO and its MW on the morphology of the Zn surfaces, the electrodes are studied using scanning electron microscopy (SEM) after cycling. The $ACE_4Zn(TFSI)_2$, $ACE_4PEO_{0.2}Zn(TFSI)_2$-1, and $ACE_4PEO_{0.2}Zn(TFSI)_2$-9 samples are analyzed after forming the internal short circuit, whereas the $ACE_4PEO_{0.2}Zn(TFSI)_2$-50 sample is analyzed after 50 cycles. The SEM images are shown in Figure 4c. The electrode cycled with the $ACE_4Zn(TFSI)_2$ sample (liquid) shows a nonuniform deposition of Zn on the electrode surface with clear signs of nucleation across the surface. These nuclei consist of Zn atoms and are not deposits of electrolyte components as confirmed by the energy dispersive X-ray (EDX) analysis, where the composition of the surface is studied by mapping them onto different elements present in the electrolyte (Figure S7). The size of nuclei and the nucleation density decreases when the PEO is introduced, and such an effect becomes more pronounced when its MW is increased. The surface morphology of the electrodes cycled with $ACE_4PEO_{0.2}Zn(TFSI)_2$-9 and $ACE_4PEO_{0.2}Zn(TFSI)_2$-50 sample differs more from the flat, pristine surface as they have undergone more cycles (46 and 50 cycles, respectively) while showing fewer signs of nucleation formation. The morphology study aligns with the stripping–plating behavior shown in Figure 4b, where PEO with higher MW is more effective in suppressing the dendrite growth. These results demonstrate that soft polymer gels can mitigate the growth of metal dendrites while preserving or even increasing the ionic conductivity of the liquid electrolyte. Following these experiments, a long-term stripping–plating study is performed on the $ACE_4PEO_{0.2}Zn(TFSI)_2$-50 cell at 40 °C. This gel demonstrates a high cyclability without short-circuiting in Zn||Zn symmetrical cell for more than 200 cycles at a current density of 0.22 mA cm^{-2} (Figure 5a). $ACE_4PEO_{0.2}Zn(TFSI)_2$-50 gel also demonstrates high reversibility and stability in a cell consisting of Zn and stainless steel (SS) foils (denoted as a Zn||SS cell). The shape of the stripping–plating curve shown in Figure 5b is stable throughout the cycles with an overpotential of 0.26 V. Figure 5c shows the coulombic efficiency of higher than 95% in the first 50 cycles for the $ACE_4PEO_{0.2}Zn(TFSI)_2$-50 electrolyte in the Zn||SS cell.

Effect of PEO in the eutectic equilibrium and its impact on the electrochemical properties

The stripping–plating tests of the gels with 1 wt% PEO showed that the UHMW polymer with MW of 5000000 g mol^{-1} exhibits the best overall performance and longevity. In addition, we verified that the addition of PEO to the $ACE_4Zn(TFSI)_2$ electrolyte does not have any noticeable impact on the anodic stability as demonstrated using the linear sweep voltammetry (LSV) shown in Figure S8. Consequently, the same plating-stripping tests are repeated at 40 °C for the gel electrolytes prepared with PEO of the same MW with varying relative concentrations of ACE, PEO, and $Zn(TFSI)_2$ (electrolytes reported in Table 2) as shown in Figure 6. All the considered electrolytes exhibit good performance in the Zn||Zn cells with the overpotentials around 0.25 V (Figure 6a).

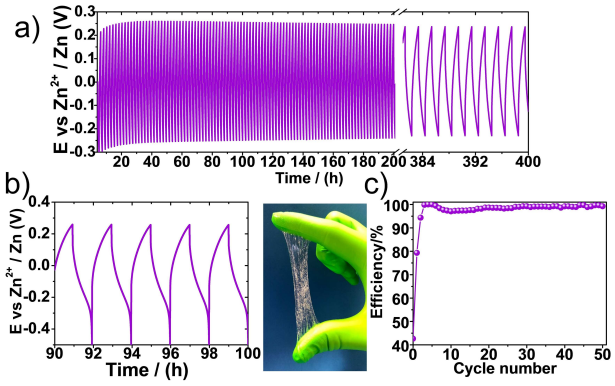

Figure 5. a) Stripping–plating behavior of $ACE_4PEO_{0.2}Zn(TFSI)_2$-50 for 200 cycles 40 °C in a symmetric Zn||Zn cell. b) Stripping–plating behavior of $ACE_4PEO_{0.2}Zn(TFSI)_2$-50 at 40 °C in a Zn||SS cell. c) Coulombic efficiency of $ACE_4PEO_{0.2}Zn(TFSI)_2$-50 electrolyte at 40 °C in Zn||SS cell.

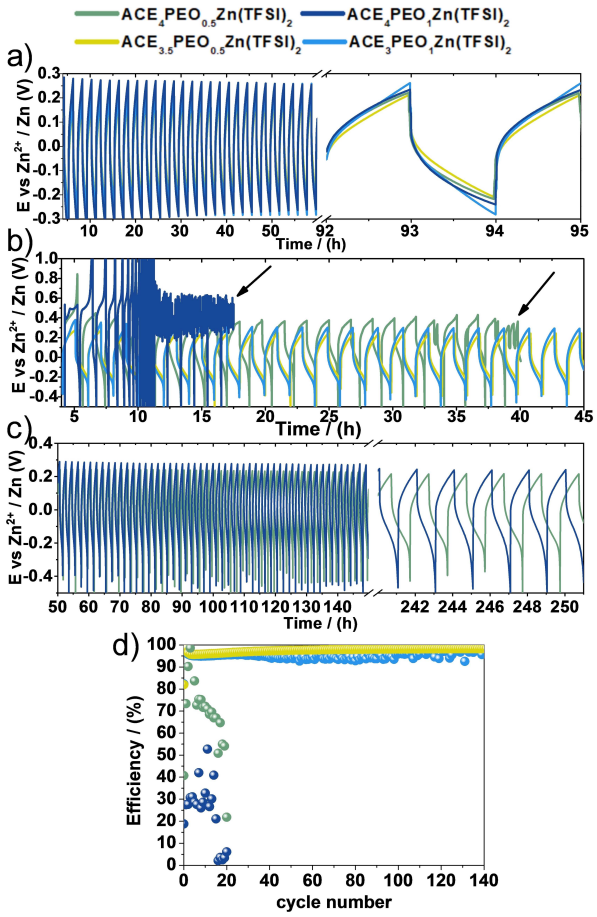

Figure 6. a,b) Stripping – plating behavior of $ACE_4PEO_{0.5}Zn(TFSI)_2$, $ACE_{3.5}PEO_{0.5}Zn(TFSI)_2$, $ACE_4PEO_1Zn(TFSI)_2$ and $ACE_3PEO_1Zn(TFSI)_2$ at 40 °C in a) Zn||Zn symmetrical cells and b) Zn||SS cells in the first 20 cycles. The arrows indicate the loss of electrochemical activity. c) Stripping – plating behavior of $ACE_{3.5}PEO_{0.5}Zn(TFSI)_2$ and $ACE_3PEO_1Zn(TFSI)_2$ at 40 °C in Zn||SS cells for an extended cycling period. d) Coulombic efficiency of $ACE_4PEO_{0.5}Zn(TFSI)_2$, $ACE_{3.5}PEO_{0.5}Zn(TFSI)2$, $ACE_4PEO_1Zn(TFSI)_2$ and $ACE_3PEO_1Zn(TFSI)_2$ at 40 °C in Zn||SS cell.

The cyclability of these electrolytes in Zn||SS cells is presented in Figure 6b. In the Zn||SS cell configuration, $ACE_4PEO_{0.5}Zn(TFSI)_2$ and $ACE_4PEO_1Zn(TFSI)_2$ lose the electrochemical activity in the early stage of the cycling test. The loss of electrochemical activity (marked with arrows in Figure 6b) is caused by the crystallization of the DES during cycling. The concentration of Zn ion in the electrolyte decreases when the Zn is plated on the SS foil, shifting the electrolyte composition out of the eutectic point. This shift leads to the precipitation of a crystalline phase. The precipitation process is faster for $ACE_4PEO_1Zn(TFSI)_2$ than for $ACE_4PEO_{0.5}Zn(TFSI)_2$, pointing once again to the critical role of PEO on the eutectic composition. The precipitation is not observed for the 1 wt% sample ($ACE_4PEO_{0.2}Zn(TFSI)_2$-50). $ACE_4PEO_1Zn(TFSI)_2$ displays a melting transition in DSC scans, whereas the presence of a crystalline phase is not detected by DSC for $ACE_4PEO_{0.5}Zn(TFSI)_2$ (Figure 3a). The $ACE_4PEO_1Zn(TFSI)_2$ formulation is already away from the eutectic point, most probably because of the scavenging of Zn^{2+} cations by complexation at the PEO chain. The Zn plating of the SS foil makes Zn^{2+} concentration in the liquid electrolyte even lower, shifting the phase equilibrium towards a higher abundance of solid species.

On the other hand, $ACE_{3.5}PEO_{0.5}Zn(TFSI)_2$ and $ACE_3PEO_1Zn(TFSI)_2$ exhibit a good cycling performance in the Zn||SS cells for at least 140 cycles (Figure 6c). The coulombic efficiencies of these two samples (Figure 6d) are very high, with more than 90% for $ACE_3PEO_1Zn(TFSI)_2$ and then 95% for $ACE_{3.5}PEO_{0.5}Zn(TFSI)_2$. The improved cycling performance of these gels compared with $ACE_4PEO_{0.5}Zn(TFSI)_2$ and $ACE_4PEO_1Zn(TFSI)_2$ corroborates well with the explanation that PEO is complexing Zn^{2+} cations and is competing with ACE in the eutectic mixture. Therefore, we suggest that the PEO should be considered as the active component of the DESs to obtain a time-stable polymer eutectogel, i.e., a eutectic liquid phase gelled by a polymer chain.

Conclusion

Gel electrolytes with pseudo-solid mechanical properties and ionic conductivity surpassing the liquid electrolyte have been prepared by a solvent-free scalable procedure. The effect of adding small amounts of PEO on physicochemical and electrochemical properties has been studied. Gels with just 1 wt% of PEO were shown to perform well for 200 cycles without the use of a separator. The effect of MW of PEO on dendrite growth mitigation has been demonstrated where the UHMW PEO outperforms the samples with lower MW. In addition, the effect of PEO on the DES structure has been studied. Ethylene oxide units of PEO act as an active component of the eutectic composition, producing the crystallization of the mixture when the PEO concentration is increased. Our results suggest that it is crucial to consider the ethylene oxide units as an active component of the eutectic composition when preparing the DESs gels to produce stable gels without crystallization.

Experimental Section

Materials

Acetamide (99%, Sigma Aldrich) and Zinc bis(trifluoromethanesulfonyl)imide ($Zn(TFSI)_2$, 99.5%, Solvionic) used to synthesize DES were opened and stored inside an argon filled glovebox. PEO of molecular weights 10^5, 9×10^5, and 5×10^6 g mol^{-1} from Sigma Aldrich used to gel the electrolytes were employed as received. Zn foil (99.9%, Goodfellow) was used for electrochemical tests.

Preparation methods

The zinc-based DESs were synthesized by mixing two solid components, ACE and $Zn(TFSI)_2$, with different molar ratios: 4:1 ($ACE_4Zn(TFSI)_2$), 3.5:1 ($ACE_{3.5}Zn(TFSI)_2$) and 3:1 ($ACE_3Zn(TFSI)_2$). They were synthesized at 80 °C with a Teflon stirrer in a heating-stirring plate. The stirring lasted 2 h until the mixture became a homogenous transparent liquid. The liquid is then slowly cooled down to room temperature (RT).

The gels have been prepared by mixing PEO in the DES, first at RT until a good powder dispersion is obtained, followed by reheating them up to 70 °C while continuously stirring to melt and dissolve the PEO. The stirring continued for another 10 min at 70 °C.[36,37] This procedure avoids the use of auxiliary solvents. The electrolytes have been characterized after a week to allow for a complete dissolution of the polymer. The preparation and storage of the DES and gels have been carried out in an argon-filled glove box with less than 1 ppm of H_2O and O_2.

Characterization

The water content in the polymers is studied as follows: first, the different MW PEO powders are introduced in the glovebox by doing three vacuum-argon cycles in the antechamber. Then 1 wt% of PEO is dissolved in anhydrous acetonitrile. The resultant polymer solutions are analyzed using a Metrohm 899 Coulometer.

DSC measurements were performed using Netzsch DSC 200 F3. Samples were placed in hermetically closed aluminum pans inside the glovebox and subjected to cooling-heating cycles at 10 °C min^{-1}, starting with cooling down to −100 °C from RT and heating from −100 °C to 150 °C. The samples were then cooled down again to −100 °C, followed by a second heating scan.

Fourier transform infrared (FTIR) spectroscopy measurements were performed using a Perkin–Elmer Spectrum-Two. The spectra are the average of 4 spectra recorded with a resolution of 4 cm^{-1}.

The rheology of the gel electrolytes is characterized by an AR–G2 rheometer using a parallel plate configuration with an upper stainless steel sandblasted plane plate of 20 mm diameter. The gel samples were placed between the Peltier and the upper plate, which were placed 1 mm apart from each other. The experiment consisted of 1 h of temperature stabilization of the sample at the experiment temperature, followed by an oscillatory frequency measurement from 0.01 rad s^{-1} to 100 rad s^{-1} applying a strain of 1%, which is within the linear viscoelastic region for these gels. The plateau modulus (G_0^N) is set as the storage (G') modulus value at the minimum of tan(δ), where tan(δ) = G''/G'. The complex viscosity (η^*) is obtained according to Equation (1):

$$\eta^* = \left[\left(\frac{G''}{\omega}\right)^2 + \left(\frac{G'}{\omega}\right)^2\right]^{\frac{1}{2}} \quad (1)$$

where G' is the storage modulus, G'' is the loss modulus and ω is the angular frequency.

Complex viscosity can be compared with the linear viscosity (η) following the Cox-Merz rule, $\eta^*(\omega) = \eta(\dot{\gamma})$, where $\dot{\gamma}$ is the strain rate. The Newtonian viscosity of the samples is obtained by fitting η with the Carreau − Yasuda equation [Eq. (S1)]. The equation and fitting curves are represented in Figure S5.

Impedance spectroscopy measurements were performed with a Biologic VMP3 potentiostat using frequencies ranging from 200 kHz to 100 mHz. The PTFE (polytetrafluoroethylene) ring spacer with internal and external diameters of 15 mm and 20 mm, respectively, was used. The samples were placed inside the ring spacer and sandwiched between two stainless steel (SS) discs inside a coin cell. The coin cells were placed in the temperature-controlled chamber, where the temperature was incremented from 10 °C to 70 °C with a 10 °C step. Each of the measurements was performed 2 h after reaching the set temperature in the chamber to allow for temperature stabilization of the samples. Ionic conductivity as a function of frequency $\sigma(\omega)$ has been obtained from the impedance values employing the dielectric theory, setting σ as the value at the frequency where tan(δ) is at its maximum. The dielectric equation employed is given in the Supporting Information [Eq. (S2)].

All electrochemical tests were performed using a Biologic VMP3 potentiostat. For the striping − plating measurements the samples were assembled in coin cells and the electrolyte was sandwiched between the two electrodes using a PTFE ring of 20 mm diameter with a 1 mm thickness with a 15 mm diameter hole as a mechanical spacer between them. Zinc foils were used as electrodes for the Zn||Zn galvanostatic stripping − plating measurements. A stainless-steel working electrode and a Zn counter electrode have been employed to study electrolyte reversibility. All electrochemical cycling tests were carried out with a current density of 0.22 mA cm^{-2}. The LSV measurements have been performed in an EL-cell with an 18 mm diameter glassy carbon working electrode and a zinc counter electrode at a scan rate of 1 mV s^{-1}. The upper and lower voltage limit was set to ±1 V. For measuring $ACE_4Zn(TFSI)_2$, a 100-micron glass fiber separator has been employed to avoid contact between electrodes. No separator has been used for the gel electrolytes.

SEM and EDX micrographs of the Zn electrode surfaces have been performed in a ZEISS EVO Scanning Electron Microscope with X-ray analysis. As these gel electrolytes are very sticky, conditioning of the electrodes has been done by immersing and sonicating in the electrodes in an ethanol bath, until the gel is dissolved. Then they are cleaned in water and again in ethanol to ensure the total elimination of the polymer.

Density functional theory simulations

The Gaussian 16 package was used to perform density functional theory (DFT) simulations to understand the interactions in the electrolytes. The M06-2X DFT functional[42] and 6–311++G(d,p) basis set[43] were employed for the optimization of the structures. The conductor-like polarizable continuum model (C-PCM)[44] was used to simulate the influence of a surrounding liquid, with the dielectric constant set to 15, which corresponds to that of DES.[45] To mimic the polymer chain, we considered dimers of PEO. The interaction energies were calculated by subtracting the energy of the generated complex from the energy of the separated molecules.

Acknowledgements

AMAPOLA H2020-EIC-FETPROACT-2019 G.A. 951902 is gratefully acknowledged.

Conflict of Interests

The authors declare no conflict of interest.

Data Availability Statement

The data that support the findings of this study are available in the supplementary material of this article.

Keywords: zinc batteries · deep eutectic solvents · polymers · gel electrolytes

[1] M. S. Whittingham, *Science* **1976**, *192*, 1126–1127.
[2] J. B. Goodenough, K. Mizushima, T. Takeda, *Jpn. J. Appl. Phys.* **1980**, *19*, 305–313.
[3] M. M. Thackeray, C. Wolverton, E. D. Isaacs, *Energy Environ. Sci.* **2012**, *5*, 7854–7863.
[4] M. Beaudin, H. Zareipour, A. Schellenberglabe, W. Rosehart, *Energy Sustain. Dev.* **2010**, *14*, 302–314.
[5] C. Grosjean, P. Herrera Miranda, M. Perrin, P. Poggi, *Renew. Sustain. Energy Rev.* **2012**, *16*, 1735–1744.
[6] X. Sun, Z. Liu, F. Zhao, H. Hao, *Environ. Sci. Technol.* **2021**, *55*, 12180–12190.
[7] S. Ponnada, M. S. Kiai, R. Krishnapriya, R. Singhal, R. K. Sharma, *Energy Fuels* **2022**, *36*, 6013–6026.
[8] J. W. Choi, D. Aurbach, *Nat. Rev. Mater.* **2016**, *1*, 16013.
[9] B. Craig, T. Schoetz, A. Cruden, C. Ponce de Leon, *Renew. Sustain. Energy Rev.* **2020**, *133*, 110100.
[10] H. Li, L. Ma, C. Han, Z. Wang, Z. Liu, Z. Tang, C. Zhi, *Nano Energy* **2019**, *62*, 550–587.
[11] M. Song, H. Tan, D. Chao, H. J. Fan, *Adv. Funct. Mater.* **2018**, *28*, 1802564.
[12] L. E. Blanc, D. Kundu, L. F. Nazar, *Joule* **2020**, *4*, 771–799.
[13] Q. Yang, Q. Li, Z. Liu, D. Wang, Y. Guo, X. Li, Y. Tang, H. Li, B. Dong, C. Zhi, *Adv. Mater.* **2020**, *32*, 2001854.
[14] H. Jia, Z. Wang, B. Tawiah, Y. Wang, C. Y. Chan, B. Fei, F. Pan, *Nano Energy* **2020**, *70*, 104523.
[15] Y. Tian, Y. An, C. Wei, B. Xi, S. Xiong, J. Feng, Y. Qian, *Adv. Energy Mater.* **2021**, *11*, 1–33.
[16] J. J. Xu, H. Ye, J. Huang, *Electrochem. Commun.* **2005**, *7*, 1309–1317.
[17] J. P. Tafur, A. J. Fernández Romero, *J. Memb. Sci.* **2014**, *469*, 499–506.
[18] B. B. Hansen, S. Spittle, B. Chen, D. Poe, Y. Zhang, J. M. Klein, A. Horton, L. Adhikari, T. Zelovich, B. W. Doherty, B. Gurkan, E. J. Maginn, A. Ragauskas, M. Dadmun, T. A. Zawodzinski, G. A. Baker, M. E. Tuckerman, R. F. Savinell, J. R. Sangoro, *Chem. Rev.* **2021**, *121*, 1232–1285.
[19] E. L. Smith, A. P. Abbott, K. S. Ryder, *Chem. Rev.* **2014**, *114*, 11060–11082.
[20] A. P. Abbott, J. C. Barron, K. S. Ryder, D. Wilson, *Chem. Eur. J.* **2007**, *13*, 6495–6501.
[21] C. Du, B. Zhao, X. B. Chen, N. Birbilis, H. Yang, *Sci. Rep.* **2016**, *6*, 1–14.
[22] N. S. Venkata Narayanan, B. V. Ashokraj, S. Sampath, *J. Colloid Interface Sci.* **2010**, *342*, 505–512.
[23] H. Qiu, X. Du, J. Zhao, Y. Wang, J. Ju, Z. Chen, Z. Hu, D. Yan, X. Zhou, G. Cui, *Nat. Commun.* **2019**, *10*.
[24] R. Puttaswamy, C. Mondal, D. Mondal, D. Ghosh, *Sustain. Mater. Technol.* **2022**, *33*, e00477.
[25] Y. Jin, K. S. Han, Y. Shao, M. L. Sushko, J. Xiao, H. Pan, J. Liu, *Adv. Funct. Mater.* **2020**, *30*.
[26] S. J. Banik, R. Akolkar, *J. Electrochem. Soc.* **2013**, *160*, D519–D523.
[27] P. Barai, K. Higa, V. Srinivasan, *Phys. Chem. Chem. Phys.* **2017**, *19*, 20493–20505.
[28] C. Monroe, J. Newman, *J. Electrochem. Soc.* **2005**, *152*, A396.
[29] S. Wei, Z. Cheng, P. Nath, M. D. Tikekar, G. Li, L. A. Archer, *Sci. Adv.* **2018**, *4*, 1–9.
[30] A. Warren, D. Zhang, S. Choudhury, L. A. Archer, *Macromolecules* **2019**, *52*, 4666–4672.
[31] Y. Zhang, A. Bahi, F. Ko, J. Liu, *Small* **2022**, *18*, 1–11.
[32] L. Wang, Z. Li, Z. Meng, Y. Xiu, B. Dasari, Z. Zhao-Karger, M. Fichtner, *Energy Storage Mater.* **2022**, *48*, 155–163.
[33] A. Mitha, A. Z. Yazdi, M. Ahmed, P. Chen, *ChemElectroChem* **2018**, *5*, 2409–2418.
[34] Q. Zhang, J. Luan, L. Fu, S. Wu, Y. Tang, X. Ji, H. Wang, *Angew. Chem. Int. Ed.* **2019**, *58*, 15841–15847.
[35] X. Zhang, Z. Pei, C. Wang, Z. Yuan, L. Wei, Y. Pan, A. Mahmood, Q. Shao, Y. Chen, *Small* **2019**, *15*, 1–9.
[36] Á. Miguel, N. García, V. Gregorio, A. López-Cudero, P. Tiemblo, *Polymers* **2020**, *12*, 1336.
[37] V. Gregorio, N. García, P. Tiemblo, *ACS Appl. Polym. Mater.* **2022**, *4*, 2860–2870.
[38] N. Pavithra, A. M. Asiri, S. Anandan, *J. Power Sources* **2015**, *286*, 346–353.
[39] E. Staunton, A. M. Christie, I. Martin-Litas, Y. G. Andreev, A. M. Z. Slawin, P. G. Bruce, *Angew. Chem. Int. Ed.* **2004**, *43*, 2103–2105.
[40] S. Chintapalli, R. Frech, B. Grady, *Polymer* **1997**, *38*, 6189–6195.
[41] G. W. Peterson, T. H. Epps, *Polymer* **2022**, *252*, 124816.
[42] Y. Zhao, D. G. Truhlar, *Theor. Chem. Acc.* **2008**, *120*, 215–241.
[43] R. Krishnan, J. S. Binkley, R. Seeger, J. A. Pople, *J. Chem. Phys.* **1980**, *72*, 650–654.
[44] V. Barone, M. Cossi, *J. Phys. Chem. A* **1998**, *102*, 1995–2001.
[45] Á. Miguel, R. P. Fornari, N. García, A. Bhowmik, D. Carrasco-Busturia, J. M. García-Lastra, P. Tiemblo, *ChemSusChem* **2020**, *13*, 5523.

Manuscript received: February 20, 2023
Revised manuscript received: March 10, 2023
Accepted manuscript online: March 14, 2023
Version of record online: May 17, 2023